Available online at www.sciencedirect.com
ScienceDirect
International Journal of Heat and Mass Transfer 50 (2007) 139–150
International Journal of HEAT and MASS TRANSFER
www.elsevier.com/locate/ijhmt

Natural convection in enclosure with heating and cooling by sinusoidal temperature profiles on one side

E. Bilgen *, R. Ben Yedder

Ecole Polytechnique, Box 6079, Centre Ville, Montreal, QC, Canada H3C 3A7

Received 13 March 2006; received in revised form 27 June 2006
Available online 1 September 2006

Abstract

A numerical study has been carried out in rectangular enclosures, which have a vertical active wall with all the other walls insulated. The equally divided active sidewall is heated and cooled with sinusoidal temperature profiles. Two cases have been considered: the first is the lower part is heated while the upper part is cooled and the second, the upper part is heated and lower part is cooled. Steady state heat transfer by laminar natural convection has been studied by numerically solving equations of mass, momentum and energy, to determine the thermal penetration in the enclosures and heat transfer as a function of Rayleigh number, the aspect ratio and the position of side heating with respect to side cooling. Rayleigh number was varied from 10^3 to 10^6 and the aspect ratio from 0.2 to 5, and the results are presented in the form of streamlines and isotherms, local and average Nusselt number, and heat penetration length. It is found that the penetration approaches to 100% at high Rayleigh numbers when the lower part is heated while the higher part is cooled. In the case of the higher part is heated and the lower part is cooled, the penetration is limited to 70% passing through maxima at Rayleigh number below 10^6.

Keywords: Natural convection; Sinusoidal temperature profile; Penetration

1. Introduction

Natural convection in fluid filled rectangular enclosures with heating from the bottom and sides has been studied extensively. We may mention among others, discrete heating in enclosures while cooling from side walls [1–4], transient heat transfer by natural convection in a square enclosure heated from part of the bottom wall, which had a uniform temperature but its magnitude varied sinusoidally with time [5], mixed convection in a channel heated by discrete heaters placed on the bottom while the opposing side was kept isothermal [6], with discrete heating from the bottom while cooled from the sides [7], turbulent natural convection–conduction in a square cavity containing a massive sidewall on which a discrete heater with constant heat flux was placed [8]. Some studies also exist, for example, with heating from the side and cooling from the top [9], or heating from below and cooling from the sides [10] as well as with heating [11,12] with various boundary conditions. This study concerns with heating and cooling from the same vertical sidewall while the others are insulated. The relevant studies in this case are those in [11,12], which we will review briefly.

Poulikakos [11] studied natural convection in rectangular enclosures isothermally heated and cooled on the same equally divided sidewall with the other walls insulated. Because of the step change in temperature at the mid-level between heated and cooled parts, there was a discontinuity problem, which was removed by assuming that the temperature at that point had an average temperature of heated and cooled parts, i.e. zero for identical absolute value in two parts. He determined heat transfer and vertical and horizontal thermal penetration as a function of Rayleigh number and the aspect ratio. Sarris et al. [12] studied numerically natural convection in a rectangular enclosure with heating from the top wall with all the others insulated.

* Corresponding author. Tel.: +1 514 340 4711x4579; fax: +1 514 340 5917.
E-mail address: bilgen@polymtl.ca (E. Bilgen).

0017-9310/$ - see front matter © 2006 Elsevier Ltd. All rights reserved.
doi:10.1016/j.ijheatmasstransfer.2006.06.027

Nomenclature

A	cavity aspect ratio, $=H/L$
c_p	heat capacity, J/kg K
g	acceleration due to gravity, m/s^2
H	cavity height, m
k	thermal conductivity, W/m K
L	cavity width, m
Nu	Nusselt number, Eq. (6)
p	pressure, Pa
P	dimensionless pressure, $=(p+\rho g y)L^2/\rho\alpha^2$
Pr	Prandtl number, $=\nu/\alpha$
Ra	Rayleigh number, $=g\beta\Delta T L^3/(\nu\alpha)$
t	time, s
T	temperature, K
T_{ref}	reference temperature, $=\frac{T(\pi/2)}{2}$, K
ΔT	temperature difference, $=T(\pi/2)-T_{\text{ref}}$, K
U, V	dimensionless fluid velocities, $=uL/\alpha$, vL/α
X, Y	dimensionless Cartesian coordinates, $=x/L$, y/L
x, y	Cartesian coordinates

Greek symbols

α	thermal diffusivity, m^2/s
β	volumetric coefficient of thermal expansion, 1/K
ν	kinematic viscosity, m^2/s
ρ	fluid density, kg/m^3
ψ	stream function
θ	dimensionless temperature, $=(T-T_{\text{ref}})/\Delta T$
τ	dimensionless time, $\alpha t/L^2$

Superscript

–	average

Subscripts

a	air
C	cold, ambient value
ext	extremum
f	fluid
H	hot, active
loc	local
max	maximum
min	minimum
o	average

Their Rayleigh number was from 10^2 to 10^8 and the aspect ratio was from 0.5 to 2. They showed that local Nusselt number at the heated wall was an increasing function of Rayleigh number and circulation strength in the cavity was an increasing function of the aspect ratio.

In this study we will analyze natural convection heat transfer in rectangular enclosures having a sidewall heated and cooled with sinusoidal temperature profiles and the other walls adiabatic. Our main objective is to determine the thermal penetration in the enclosure and heat transfer as a function of Rayleigh number, the aspect ratio and the position of side heating with respect to side cooling. We see from the literature review that the case of heating with sinusoidal temperature profile on the sidewall has not been addressed. This case has applications and implications especially for shallow enclosures in which thermal penetration has certain importance in industrial processes and furnaces.

2. Problem and mathematical model

2.1. Problem definition

A schematic of the two dimensional system, and the coordinates and boundary conditions are shown in Fig. 1. The cavity is differentially heated and cooled along a single vertical side, with other sides insulated. Sinusoidal temperature distributions are applied on the vertical side as

$$\left.\begin{aligned} T(y) &= T_{\text{ref}} \pm \Delta T \sin\left(2\pi\tfrac{y}{H}\right) \\ \theta &= \tfrac{T-T_{\text{ref}}}{\Delta T} = \pm\sin(2\pi Y) \end{aligned}\right\} \quad (1)$$

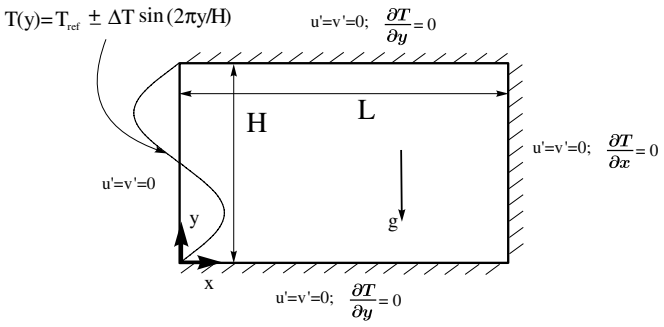

Fig. 1. Schematic of the rectangular enclosure, the coordinate system and boundary conditions.

where positive sign is for heating from the lower half and negative sign for heating from the upper half.

2.2. Mathematical model

Following assumptions are made: the flow is laminar of an incompressible Newtonian fluid and two-dimensional, there is no viscous dissipation, the gravity acts in the vertical direction, fluid properties are constant and fluid density variations are neglected except in the buoyancy term (the Boussinesq approximation), and radiation heat exchange is negligible.

The continuity, momentum and energy equations are written. Using non-dimensional variables defined in the nomenclature, the non-dimensional governing equations are obtained as

$$\frac{\partial U}{\partial X}+\frac{\partial V}{\partial Y}=0 \tag{2}$$

$$\frac{\partial U}{\partial \tau}+U\frac{\partial U}{\partial X}+V\frac{\partial U}{\partial Y}=-\frac{\partial P}{\partial X}+Pr\nabla^2 U \tag{3}$$

$$\frac{\partial V}{\partial \tau}+U\frac{\partial V}{\partial X}+V\frac{\partial V}{\partial Y}=-\frac{\partial P}{\partial Y}+Pr\nabla^2 V+Ra\,Pr\,\theta \tag{4}$$

$$\frac{\partial \theta}{\partial \tau}+U\frac{\partial \theta}{\partial X}+V\frac{\partial \theta}{\partial Y}=\nabla^2\theta \tag{5}$$

The steady-state solutions are obtained from unsteady-state equations, Eqs. (2)–(5). The local, average and normalized average Nusselt numbers are calculated respectively as

$$\left.\begin{aligned} Nu_{\mathrm{loc}} &= -\tfrac{\partial\theta}{\partial X}\\ \overline{Nu} &= \textstyle\int_0^A Nu_{\mathrm{loc}}\,\mathrm{d}Y\\ Nu &= \tfrac{\overline{Nu}_{Ra}}{\overline{Nu}_{Ra=0}} \end{aligned}\right\} \tag{6}$$

where $\overline{Nu}_{Ra}$ is the Nusselt calculated for $Ra>0$ and $\overline{Nu}_{Ra=0}$ is calculated for $Ra=0$, i.e. for pure conduction, from the second equation of Eq. (6).

The stream function is calculated from its definition as

$$U=-\frac{\partial\psi}{\partial Y},\quad V=\frac{\partial\psi}{\partial X} \tag{7}$$

where ψ is zero on the solid surfaces and the streamlines are drawn by $\Delta\psi=(\psi_{\max}-\psi_{\min})/n$ with $n=$ number of increments.

2.3. Boundary conditions

The boundary conditions of the system are shown in Fig. 1. Velocities are zero on all solid surfaces, normal pressure gradient are zero on all solid surfaces at the outside boundaries. On the adiabatic boundaries, temperature gradient is zero. On the left vertical boundary, a sinusoidal temperature is applied, in the first case (case A), heated on lower half while cooled on the upper half, and in the second case (case B), the inverse. Thus,

$$\left.\begin{aligned} &\text{On all solid boundaries:}\quad U=V=0\\ &\text{On } X=0,\quad 0<Y<A:\quad \theta=\pm\sin(2\pi Y)\\ &\text{On } Y=0,\ A,\quad 0<X<1:\quad \tfrac{\partial\theta}{\partial Y}=0\\ &\text{On } X=1,\ Y=0 \text{ to } A:\quad \tfrac{\partial\theta}{\partial X}=0 \end{aligned}\right\} \tag{8}$$

3. Numerical technique

The numerical method used to solve Eqs. (2)–(5) is the SIMPLER (Semi-Implicit Method for Pressure Linked Equations Revised) algorithm [13]. The computer code based on the mathematical formulation presented above and the SIMPLER method were validated earlier [14] and also in this study.

Table 1
Comparison of results for natural convection in a differentially heated square cavity

Ra	Benchmark [15] (60 × 60)		de Vahl Davis [15] (60 × 60)		Wan et al. [16] (FEM)	This study (60 × 60)	
	Nu_o	$\Psi_{\max}$	Nu_o	$\Psi_{\max}$	Nu_o	Nu_o	$\Psi_{\max}$
10^3	–	1.117	1.117	1.117	–	1.117	1.177
10^4	2.238	–	2.242[a]	–	2.254	2.246	5.076
10^5	4.509	9.612	4.531	9.667	4.598	4.532	9.623
10^6	8.817	16.750	9.035	17.113	8.976	8.871	16.983
10^7	–	–	–	–	16.656	16.845	31.018

[a] (40 × 40).

Validation was carried out with respect to the benchmark case in a square cavity [15] as well as to those benchmark quality results in the literature [15,16]. It is calculated for Ra from 10^3 to 10^7 with the mesh size of 60 × 60. Average Nusselt number Nu_o and the maximum stream function $\Psi_{\max}$ at Ra are compared in Table 1. It is seen that the agreement is excellent: The maximum deviation in Nusselt number obtained by the code with reference to the benchmark solution [15] is 0.5% for $Ra=10^5$ and 0.6% for $Ra=10^6$, while that in $|\Psi_{\max}|$ is 0.11% and 1.4% respectively. With respect to the solution of de Vahl Davis in [15] and that of Wan et al. [16], they are equally in good concordance. As a further check, the average Nusselt numbers at the hot and cold walls were compared, which showed a maximum difference of about 0.5% in all runs.

The present code was tested also to simulate the case studied by Sarris et al. [12]. We calculated local Nusselt number for the square cavity at $Ra=10^5$, 10^7 and 10^8 and compared with the data from their Fig. 6. For $Ra=10^5$ and 10^7, we found the same values and for $Ra=10^8$, the maximum deviation was 0.017% at positions near the vertical boundaries at $X=0.05$ and 0.95.

Uniform grid in X and Y direction were used for all computations. Grid convergence was studied for the case of $A=1$ with grid sizes from 40 × 40 to 120 × 120 at $Ra=10^5$. Grid independence was achieved with grid size of 80 × 80 within 0.3% in Nusselt number and 0.6% in extremum stream function. Similar tests were done with the cavities having A from 0.2 to 5, and found that the grid size was satisfactory with the following grids: 81 × 21 for $A=0.2$ to 0.5, 41 × 81 for $A=2$, and 21 × 81 for $A=4$ to 5. Using a system with 2.0 GHz clock speed, a typical execution time, at $Ra=10^5$ for example, was 310 s.

A converged solution was obtained by iterating in time until variations in the primitive variables between subsequent time steps were very small:

$$\Sigma(\phi_{i,j}^{\mathrm{old}}-\phi_{i,j})<10^{-4} \tag{9}$$

where ϕ stands for U, V, and θ.

Within the same time step, residual of the pressure term was less than 10^{-3} [13]. In addition, the accuracy of the solution was double-checked using the energy conservation on the domain to ensure it was less than 10^{-4}.

4. Results and discussion

The rectangular cavities with aspect ratio, $A = 0.2$, 0.25, 0.50, 1, 2, 4 and 5 were studied at Rayleigh number from 10^3 to 10^6. Two cases were considered, one with lower half heated, upper half cooled by a sinusoidal temperature profile (designated as Case A and shown in Fig. 1) and the other with upper half heated, lower half cooled by the same temperature profile (designated as case B). Prandtl number was 0.7. We will first present Case A in which the lower half is heated and upper half is cooled as in Fig. 1.

4.1. Case A: Lower half heated

Using Eqs. (6) and (7), the flow and temperature fields are produced, average Nusselt number is calculated, local Nusselt numbers along the active side wall as well as at $Y = 0.5$ in the X direction are calculated. First, we will present typical flow and temperature fields, and discuss the mechanism of heat transfer. Then we will present thermal penetration in the cavity and finally the heat transfer.

4.1.1. Flow and temperature fields

They are presented at Rayleigh from 10^3 to 10^6 in Fig. 2 for a square enclosure, in Fig. 3 for tall enclosures with aspect ratio of 2 and 5, and in Fig. 4 for shallow enclosures with aspect ratio of 0.5 and 0.2. We can see that in all cases, the flow and temperature fields are symmetric at $Y = 0.5$ plane. Indeed, some cases were computed using half of the domain and found exactly the same results with those presented in these figures. The mechanism of heat transfer is by a single cell rotating in clockwise direction in the lower half, driven by the hot wall. The heat is transfered to the upper half along the symmetry plane at $Y = 0.5$, as a result of which a counter clockwise rotating single cell is formed. This cell is cooled at the cold wall, which also has a sinusoidal temperature profile.

Fig. 2 shows for $A = 1$, flow and temperature fields for Ra from 10^3 to 10^6 in (a) to (d) respectively. The strength of the circulation $|\Psi_{ext}|$ is 0.1813 ($X = 0.3000$, $Y = 0.2750$) at $Ra = 10^3$, it becomes 1.8718 ($X = 0.3000$, $Y = 0.2875$) at $Ra = 10^4$, 8.5666 ($X = 0.4750$, $Y = 0.3000$) at $Ra = 10^5$, and 27.0699 ($X = 0.6500$, $Y = 0.2750$) at $Ra = 10^6$. Thus, as expected, it increases with Rayleigh number and the coordinate shifts from close to the hot wall towards inside, i.e. the flow penetrates into the cavity more and more with increasing Rayleigh number, which is also clearly visible in the flow field figures. As a consequence, the temperature field also follows the same trend and the temperature gradient along the symmetry plane is increased with increasing Rayleigh number.

For $A = 2$, we see in Fig. 3(a) that the appearance of the flow field is the same at Rayleigh from 10^3 to 10^6 in (i) to (iv) respectively, although $|\Psi_{ext}|$ has obviously increased from 1.023 to 23.2894. The horizontal as well as vertical penetration of flow seems to be the same. The isotherms on the right show that as Rayleigh increases, the thermal penetration becomes more vigorous with higher temperature gradient along the symmetry plane, i.e. increased heat transfer from the lower to the upper half of the enclosure. For $A = 5$ in Fig. 3(b), the streamlines show that the vertical penetration is incomplete. It is about 85% at $Ra = 10^3$ and gradually increasing to about 90% at 10^6 in Fig. 3(b-iv). Beyond the penetration limit, although a weak cell is visible at low Rayleigh numbers, it also disappears at higher Rayleigh numbers and the fluid is stagnant. $|\Psi_{ext}|$ for this case varies from 0.0071 at $Ra = 10^3$ to 8.1981 at 10^6 in (b-i) to (b-iv). The isotherms show in these regions that the heat transfer is conduction dominated.

Flow and temperature fields in the lower half of the shallow enclosures are presented in Fig. 4(a) for $A = 0.5$ and in Fig. 4(b) for $A = 0.2$. Ra is from 10^3 to 10^6 corresponding respectively to (i) to (iv). In Fig. 4(a) at $Ra = 10^3$, the circulation strength is weak with $|\Psi_{ext}| = 0.1859$ at $X = 0.3000$, $Y = 0.2750$. As Rayleigh increases to 10^4, its location does not change much but $|\Psi_{ext}| = 1.8874$ and the penetration into the cavity is increased. Further increase in Rayleigh results gradually in full penetration of flow into the cavity, with $|\Psi_{ext}|$ from 8.2724 ($X = 0.4750$, $Y = 0.3000$) at $Ra = 10^5$ to 22.5723 ($X = 1.5$, $Y = 0.2750$) at 10^6. Isotherms for this case show that temperature gradient at the hot wall is an increasing function of Rayleigh number. The temperature gradient at the symmetry plane is very small for $Ra = 10^3$ and it gradually increases with Rayleigh number implying that the length of the symmetry plane participating in heat transfer to the upper half is increased. In the case of shallower enclosure with $A = 0.2$ in Fig. 4(b), we can see the flow and temperature fields do not penetrate completely even at $Ra = 10^6$, in which case $|\Psi_{ext}| = 21.2384$ at ($X = 1.0000$, $Y = 0.3250$).

We expect that the local Nusselt number with the sinusoidal temperature profile on the wall will have a different variation from that of an isothermal case. Typical local Nusselt number on the heated part of the active sidewall is shown in Fig. 5 for $A = 0.25$ and 0.50. Nu_{loc} profiles are for Ra from 10^3 to 10^6. Nu_{loc} is positive when heat is transfered into the enclosure and negative when it is from the enclosure to environment. Following the sinusoidal variation of the wall temperature, at the lower and upper parts of the active wall, the temperature gradient is not favorable for heat transfer from the wall to the enclosure air. Thus, generally, at all Rayleigh numbers, heat is transfered from the enclosure to environment at these parts, particularly at the lower part, since the returning fluid is relatively warmer than the wall temperature. This mechanism becomes less important as Ra is increased, since the convection and hence the heat transfer to the upper part in the enclosure is increased. For low Rayleigh numbers, at $Ra < 10^4$ the heat transfer at the upper part is from the wall into the enclosure but as Ra increases, since the fluid becomes much warmer than the that of the upper part of the wall, the heat transfer becomes from the enclosure to the environment. The same is observed for the aspect ratio

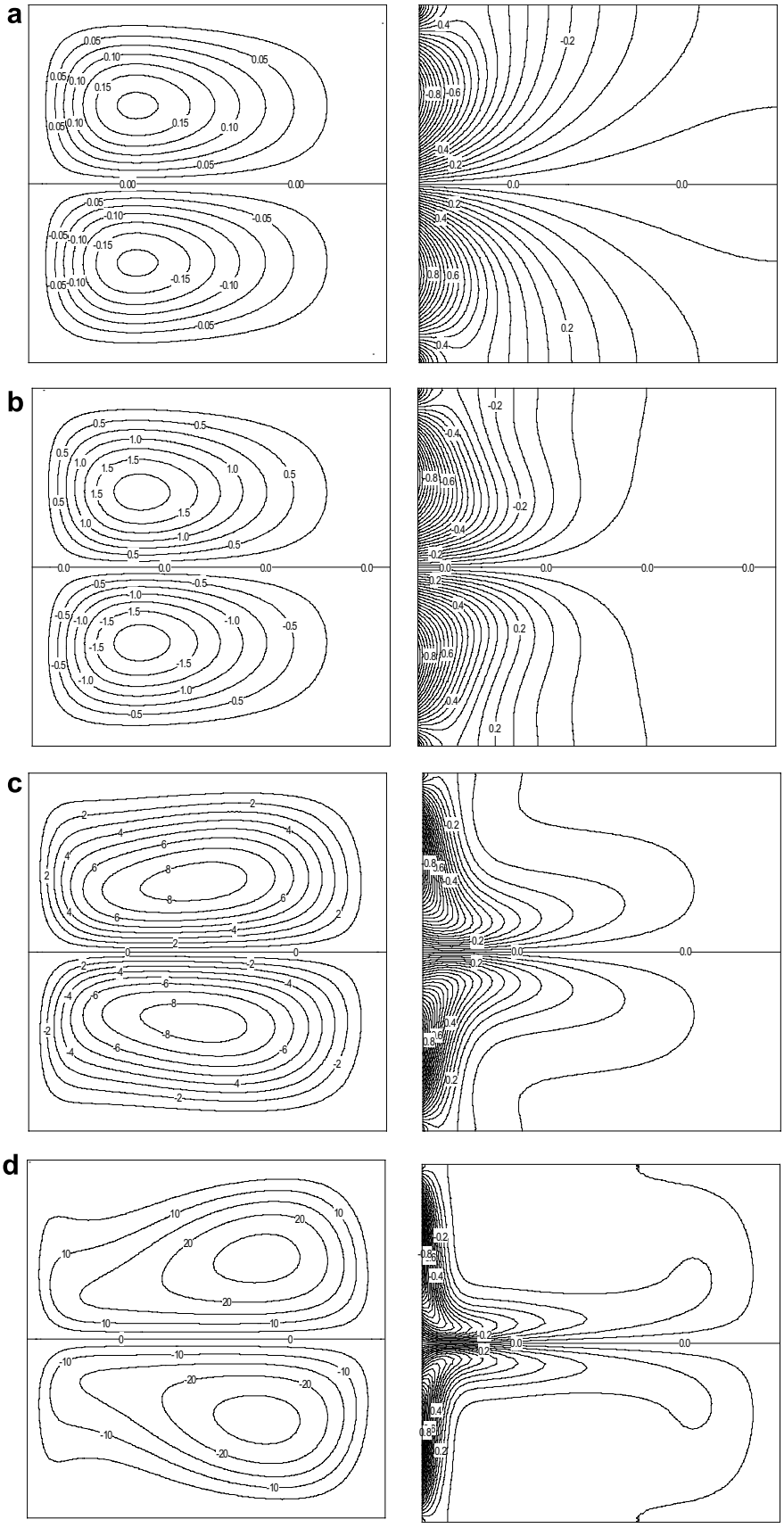

Fig. 2. Flow (the left figures) and temperature (the right figures) fields for $A = 1$ and various Rayleigh numbers: (a) $Ra = 10^3$, (b) $Ra = 10^4$, (c) $Ra = 10^5$ and (d) $Ra = 10^6$.

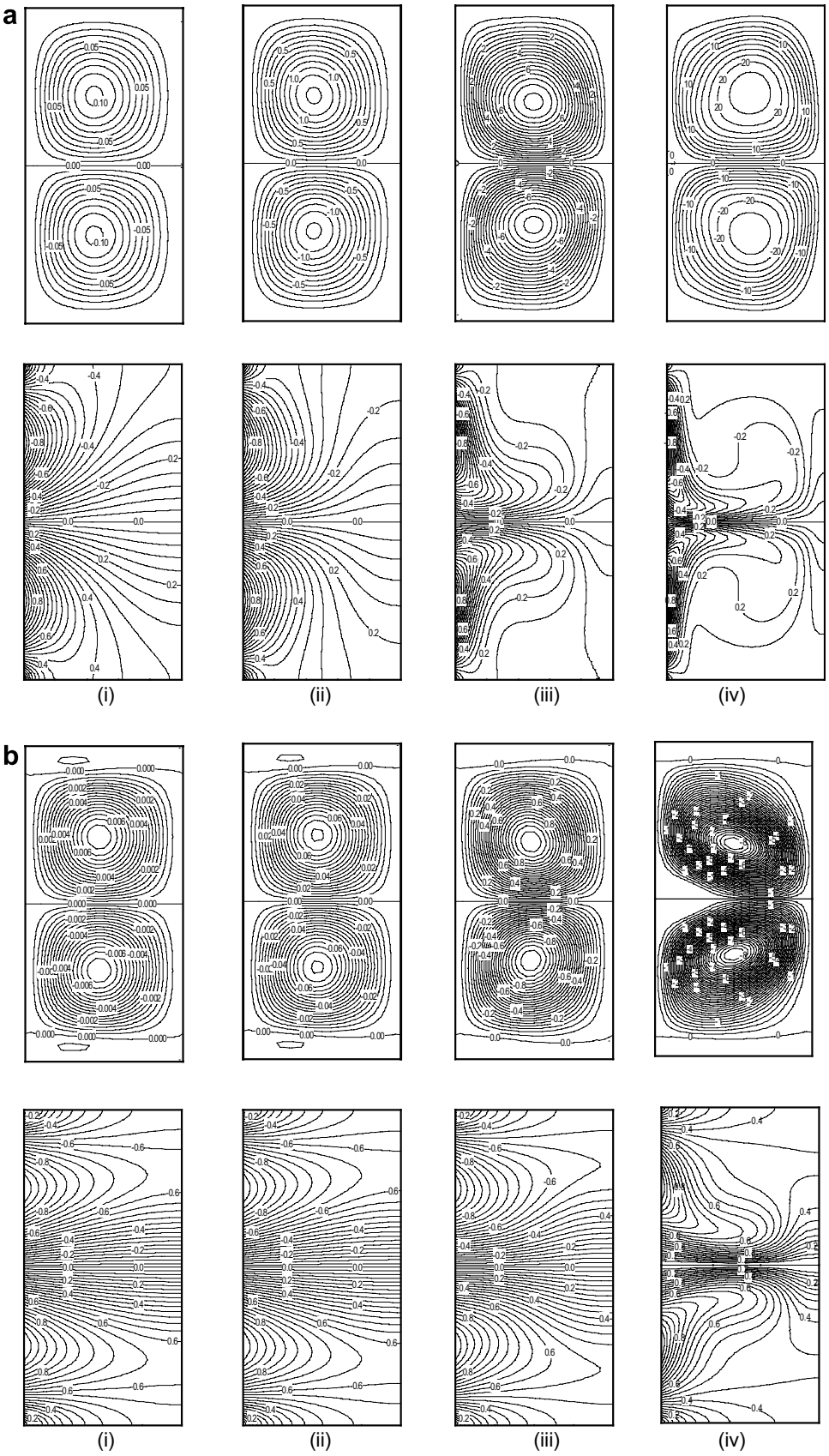

Fig. 3. Flow (the upper figures) and temperature (the lower figures) fields for (a) $A = 2$: (i) $Ra = 10^3$, (ii) $Ra = 10^4$, (iii) $Ra = 10^5$ and (iv) $Ra = 10^6$; (b) $A = 5$ (the scale is changed in the X direction): (i) $Ra = 10^3$, (ii) $Ra = 10^4$, (iii) $Ra = 10^5$ and (iv) $Ra = 10^6$.

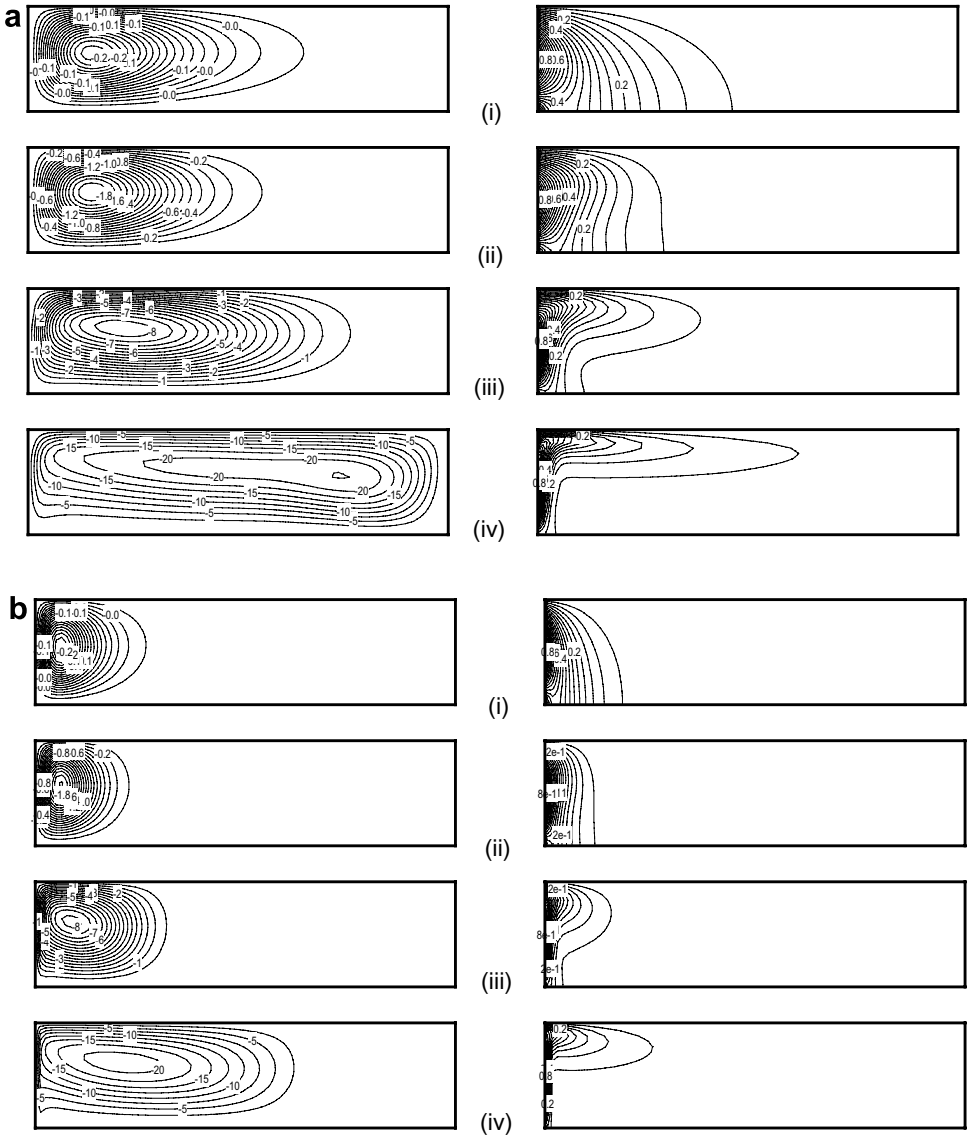

Fig. 4. Flow (the left figures) and temperature (the right figures) fields in the lower half of the enclosure for (a) $A = 0.5$: (i) $Ra = 10^3$, (ii) $Ra = 10^4$, (iii) $Ra = 10^5$ and (iv) $Ra = 10^6$, and for (b) $A = 0.2$: (i) $Ra = 10^3$, (ii) $Ra = 10^4$, (iii) $Ra = 10^5$ and (iv) $Ra = 10^6$.

of $A = 0.25$ and 0.50. Although the strength of local Nusselt number changed with Rayleigh number and the aspect ratio, in all the other cases, with A from 0.20 to 5, a similar mechanism of heat transfer in and out of the enclosure was observed. We observed also that in the upper as well as in the lower half of the enclosure the local Nusselt profiles were symmetric at $Y = 0.5$ plane, and exactly the same phenomena existed in the upper half of the enclosure, where the fluid is cooled down along the active wall with heat transfer from the environment into the enclosure in the upper and lower parts of the active wall.

4.1.2. Thermal penetration

For tall enclosures, it can be determined approximately from the flow and temperature fields. The same cannot be easily done for shallow enclosures. Following our discussion regarding the mechanism of heat transfer through the symmetry plane, there will be heat transfer between lower and upper parts as long as there is a heat transport by the cells in either half due to temperature gradients along the symmetry plane at $Y = 0.5$. For this reason, to determine thermal penetration length in this case, we traced the local Nusselt number along the symmetry plane and determined the point where local Nusselt number becomes zero.

The case with Rayleigh at 10^5 and 10^6 is presented in Fig. 6. We can see clearly in the upper figure for $Ra = 10^5$ that, the thermal penetration is $X = 0.2648/0.2 = 1.324$ or 26.48% for $A = 0.2$, $X = 0.6648/0.5 = 1.330$ or 66.50% for $A = 0.5$ and $X \approx 1$, a complete penetration for $A = 1$. Similarly for $Ra = 10^6$ in the lower figure, the thermal penetration is determined as $X = 0.4594/0.2 = 2.297$ or 45.94%

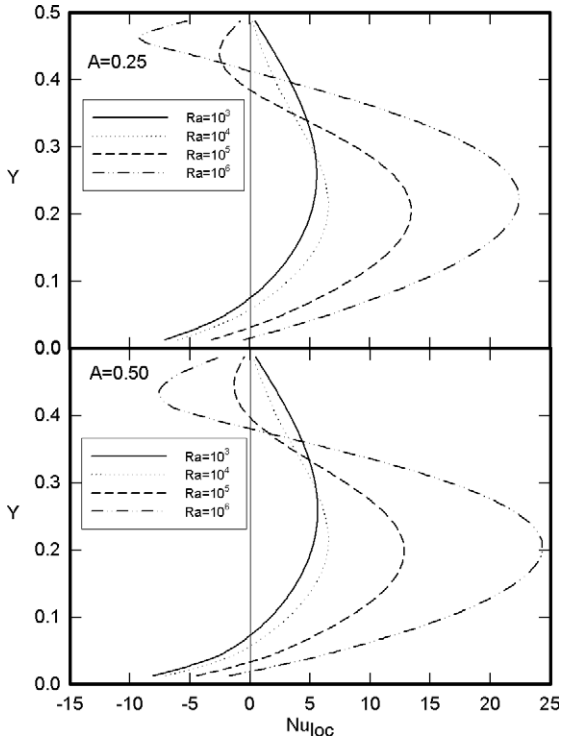

Fig. 5. Local Nusselt number at ($X = 0$, Y) along the heated wall in the lower half of the enclosure (case A) for $A = 0.25$ (the upper figure) and $A = 0.50$ (the lower figure) for various Rayleigh numbers.

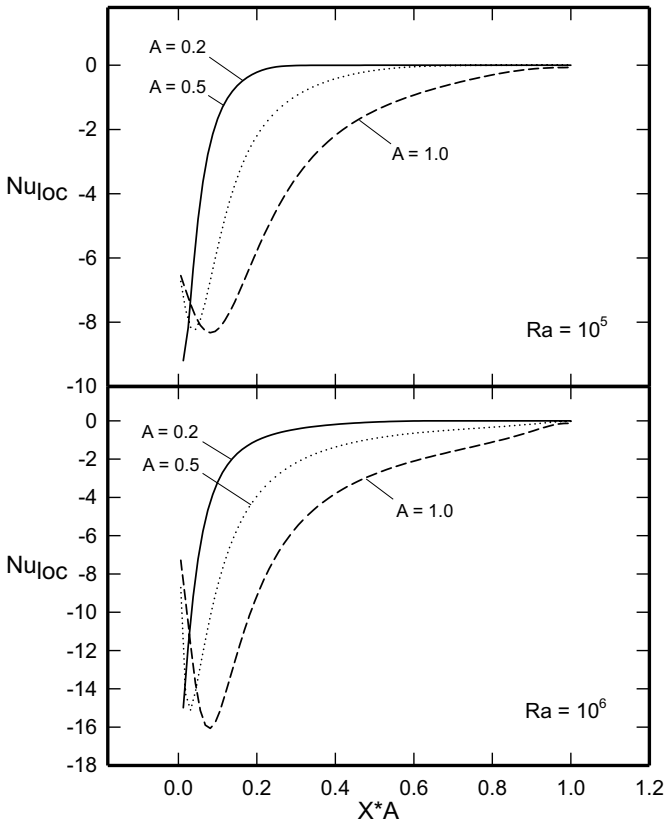

Fig. 6. Local Nusselt number at (X, $Y = 0.5$) along the symmetry plane as a function of XA for various aspect ratios and $Ra = 10^6$.

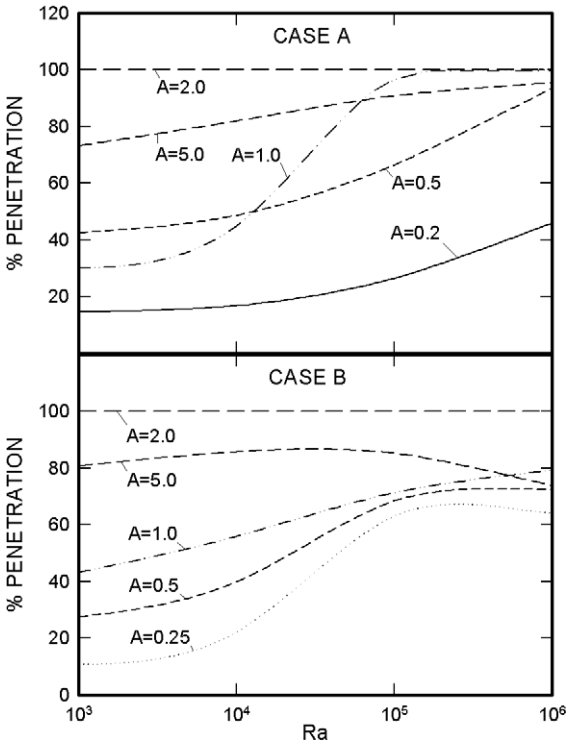

Fig. 7. Thermal penetration in the enclosure as a function of Rayleigh number and for various aspect ratios. Percentage thermal penetration is in X direction for shallow enclosures and in Y direction in tall enclosures.

for $A = 0.2$, $X = 0.935/0.5 = 1.870$ or 93.50% for $A = 0.5$ and $X \approx 1$, a complete penetration for $A = 1$. Percentage thermal penetration for case A obtained for tall and shallow enclosures is presented as a function of Rayleigh number in upper part of Fig. 7. In general, the thermal penetration is an increasing function of Rayleigh number with the exception of the case with $A = 2$. In enclosures with aspect ratio from 1 to 5, it appears that an optimum thermal penetration exists at low Rayleigh numbers and as Ra increases, the percentage thermal penetration approaches towards 100%. For shallow enclosures, percentage thermal penetration is an increasing function of the aspect ratio and Rayleigh number. These results are expected in view of the flow and temperatures fields presented and discussed earlier.

4.1.3. Heat transfer

Normalized average Nusselt number on the hot or cold wall is calculated from the last equation of Eq. (6) and presented in the upper figure of Fig. 8 for case A. We can observe that heat transfer is conduction dominated at low Rayleigh numbers up to about 10^4 for all cases. At higher Rayleigh numbers, the convection becomes dominant except for tall enclosures, for which convection is suppressed further up to about 10^5, thereafter convection becomes dominant. Generally, in convection dominated regime, heat transfer is enhanced with increasing Rayleigh number and decreasing aspect ratio. These results are expected in view of the flow and temperature fields presented and discussed in Figs. 2–4.

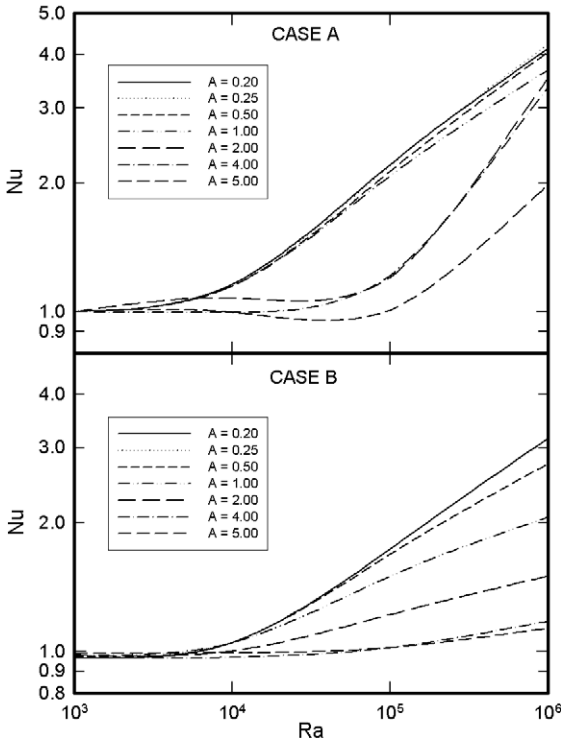

Fig. 8. Normalized average Nusselt number as a function of Rayleigh number with the aspect ratio as a parameter. Case A is when heated in the lower half of the active wall and case B is when heated in the upper half.

4.2. Case B: Upper part heated

From the computation point of view this case does not represent any instability problems at high Rayleigh numbers, since the fluid is heated from the upper half of the enclosure. However, it is more complicated than case A, because the fluid heated on the hot wall turns at the end of it and moves along the upper adiabatic wall, then vertical adiabatic wall before transferring its heat at the symmetry plane to the lower cell.

4.2.1. Flow and temperature fields

We will present, similarly but briefly, the flow and temperature fields and heat transfer. Fig. 9 presents (a) flow and temperature fields for tall enclosures with $A = 1$, 2 and 4 in (i) to (iii) respectively, at $Ra = 10^6$, and (b) for shallow enclosures with $A = 1$, 0.5 and 0.2 in (i) to (iii) respectively, at $Ra = 10^5$. Striking difference with respect to case A is that the strength of the circulation is much weaker and the thermal penetration is reduced considerably. For square and tall enclosures in Fig. 9(a), $|\Psi_{ext}|$ is 8.2913 ($X = 0.1625$, $Y = 0.8375$) for $A = 1$, 6.4780 ($X = 0.1625$, $Y = 0.8250$) for $A = 2$ and 3.6401 ($X = 0.1125$, $Y = 0.7750$) for $A = 4$ all at $Ra = 10^6$. The location of $|\Psi_{ext}|$ is very close to the active side wall for all aspect ratios. Of course, as the enclosure is taller, the coordinate of $|\Psi_{ext}|$ is closer to the active side wall. For square and shallow enclosures in Fig. 9(b), the situation is similar with amplifications: $|\Psi_{ext}|$ is 4.0202 ($X = 0.2125$, $Y = 0.7750$) for $A = 1$, 4.8159 ($X = 0.2500$, $Y = 0.7500$) for $A = 0.5$ and 4.9751 ($X = 0.2500$, $Y = 0.7500$) for $A = 0.2$, which shows that the strength of circulation is almost constant and the coordinate of $|\Psi_{ext}|$ is almost at the same with decreasing aspect ratio. This shows that thermal penetration is more difficult in case B than case A. In fact, the isotherms show that for the cases in both figures, the temperature gradients are not appreciable after certain distance, which implies that heat transfer between the sections is negligibly small.

4.2.2. Thermal penetration

They are calculated using the same technique as in case A, i.e. the identification of the point where the temperature gradient becomes negligibly small. The results as percentage thermal penetration as a function of Rayleigh number for various aspect ratios are presented in the lower part of Fig. 7. Similar to the results of case A, percentage thermal penetration is an increasing function of the aspect ratio and Rayleigh number and there exists an optimum aspect ratio at $A = 2$. The striking difference from case A is that percentage thermal penetration is generally smaller and approaches to about 70% at $Ra = 10^6$. It appears also that at Rayleigh number greater than 10^6 this trend may continue and the percentage penetration may even become smaller, although this point has not been ascertained in this study.

4.2.3. Heat transfer

Normalized average Nusselt number on the hot or cold wall is calculated by Eq. (6) and presented in the lower figure of Fig. 8 for case B. Heat transfer is conduction dominated at low Rayleigh numbers up to about 10^5 for tall enclosures and up to 10^4 for all. As the aspect ratio decreases towards $A = 1$, the convection becomes gradually dominant. For shallow enclosures, as the aspect ratio decreases further, heat transfer increases with increasing Ra number. Following our observation regarding Fig. 9(b), the convection is suppressed considerably for this case. As expected, in convection dominated regime, heat transfer is enhanced with increasing Rayleigh number and decreasing aspect ratio.

Local Nusselt number profiles on the active wall for $A = 0.50$ and 0.20 are shown in Fig. 10 and those for $A = 2$ and 4 in Fig. 11. In these figures, the profiles are traced for Y from 0 to 1. As discussed earlier, we can see clearly that the local Nusselt number profiles along Y are symmetric with respect to the symmetry plane dividing hot and cold parts of the enclosure at $Y = 0.5$. Fig. 10 shows that the mechanism discussed regarding Fig. 5 for case A is also applicable in this case. In comparing Figs. 5 and 10, for example, we notice that although there is heat transfer from the enclosure to the environment near the horizontal walls, it is not the case at the symmetry plane at $Y = 0.5$, where Fig. 10 shows that local Nusselt number becomes zero at all Ra numbers. Heat is transfered from enclosure to environment near at $Y = 1$ level, because the fluid is warmer than the wall. At the symmetry plane level, heat is transfered completely from the upper half to the

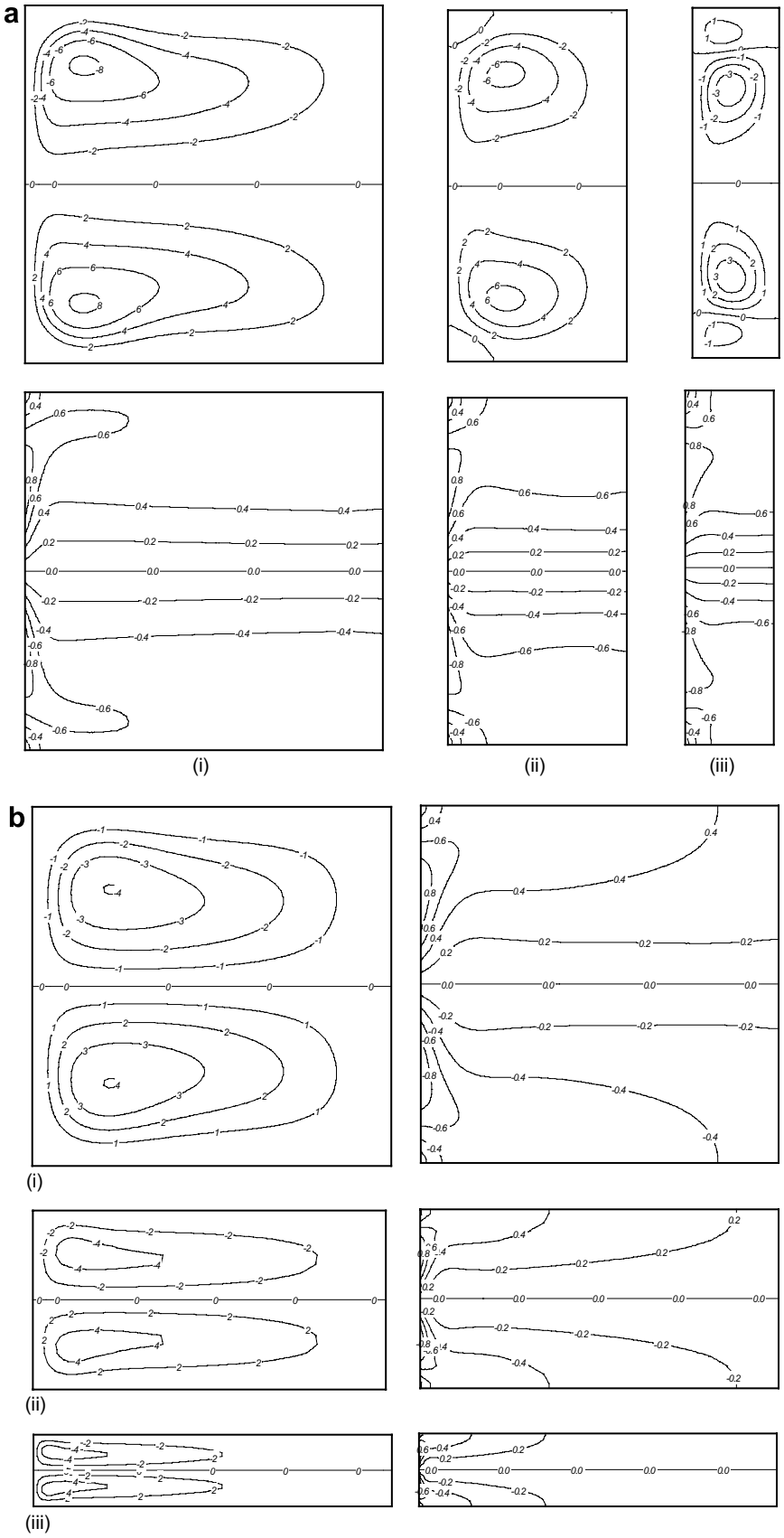

Fig. 9. Flow and temperature fields for case B (the wall is heated in the upper half while cooled in the lower half). (a) The flow field is in the upper part and the temperature field in the lower, and for $Ra = 10^6$: (i) $A = 1$, (ii) $A = 2$ and (iii) $A = 4$. (b) The flow field is on the left and the temperature field on the right, and for $Ra = 10^5$: (i) $A = 1$, (ii) $A = 0.5$ and (iii) $A = 0.2$.

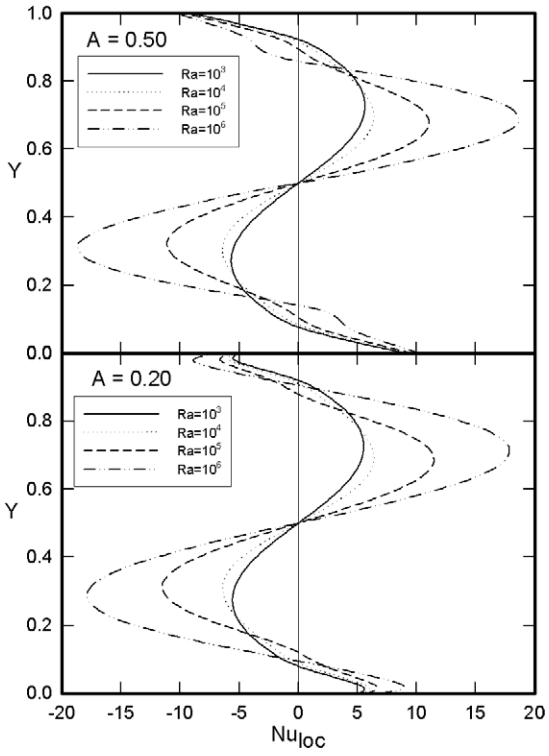

Fig. 10. Local Nusselt number at ($X = 0$, Y) along the heated and cooled sections (case B) for $A = 0.50$ (the upper figure) and $A = 0.20$ (the lower figure) for various Rayleigh numbers.

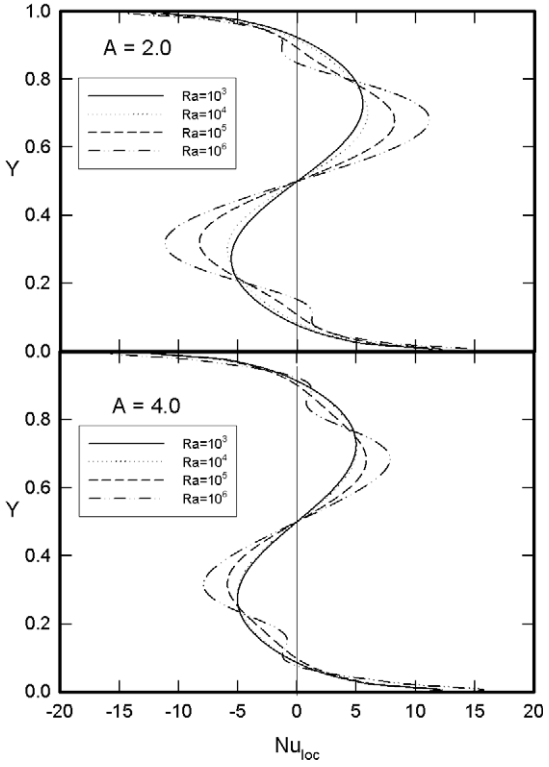

Fig. 11. Local Nusselt number at ($X = 0$, Y) along the heated and cooled sections (case B) for $A = 2$ (the upper figure) and $A = 4$ (the lower figure) for various Rayleigh numbers.

lower and there is no heat transfer to the environment. It is also noticed for $A = 0.5$ in both figures that the strength of Nu_{loc} for case B is reduced considerably with respect to case A. In tall enclosure case in Fig. 11, similar observations are made. In this case, the strength of heat transfer near horizontal boundaries is increased and following Fig. 9(a), the formation of the secondary counter rotating cell is discernible at $Ra = 10^6$ and its effect on Nu_{loc} profile.

5. Conclusions

A numerical study has been carried out in rectangular enclosures, which have a vertical active wall and all other walls are insulated. The equally divided active sidewall is heated and cooled with sinusoidal temperature profiles. Two cases have been considered: the first is the lower half is heated while the upper half is cooled and the second, the upper half is heated and lower half is cooled. The influence of Rayleigh number, of the aspect ratio, the position of the heated part on the heat transfer characteristics is examined. In view of the results and discussion presented, the following main conclusions have been drawn.

- The flow and temperature fields are symmetric with respect to the horizontal plane equally dividing lower heated (cooled) and upper cooled (heated) sections.
- The local Nusselt number at the active wall is governed by the sinusoidal temperature profile. For low wall temperatures, depending on the sign of the temperature gradient in the horizontal direction, the local Nusselt number may become negative (positive) at the heated (cooled) section, i.e. the heat transfer from the enclosure to the environment (from the environment to the enclosure).
- The normalized Nusselt number or heat transfer is dominated by conduction at low Rayleigh numbers and by convection at high Rayleigh numbers. The influence of the smaller aspect ratio is to increase the heat transfer.
- When the heated section is in the lower half of the enclosure, the heat transfer is higher, especially at high Rayleigh numbers, than that in which the heated section is at the upper half of the enclosure.
- The thermal penetration is a function of the aspect ratio and Rayleigh number. Generally, it approaches to 100% at high Rayleigh numbers when the lower half heated and the upper half cooled (case A) while about 70% when the upper half is heated and the lower half is cooled (case B). In addition, in the latter case it appears that the thermal penetration goes through maxima at lower than $Ra = 10^6$, perhaps indicating that at still higher Rayleigh numbers, if this trend continues, the percentage thermal penetration may become even smaller.

Acknowledgement

Financial support by Natural Sciences and Engineering Research Council of Canada is acknowledged.

References

[1] E. Ntibarufata, M. Hasnaoui, P. Vasseur, E. Bilgen, Numerical study of natural convection in habitat with direct gain passive window systems, Renew. Energy 4 (1994) 33–40.
[2] R.B. Chinnakotla, D. Angirasa, L. Mahajan, Parametric study of buoyancy induced flow and heat transfer from L shaped corners with asymmetrically heated surfaces, Int. J. Heat Mass Transfer 39 (1996) 851–865.
[3] E.K. Turkoglu, N. Yucel, Effect of heater and cooler locations on natural convection in square cavity, Numer. Heat Transfer A 27 (1995) 351–358.
[4] N.H. Saeid, Y. Yaacob, Natural convection in a square cavity with spacial side wall temperature variation, Numer. Heat Transfer A 49 (2006) 683–697.
[5] E.K. Lakhal, M. Hasnaoui, P. Vasseur, E. Bilgen, Natural convection in a square enclosure heated periodically from part of the bottom wall, Numer. Heat Transfer A 27 (1995) 319–333.
[6] E. Bilgen, X. Wang, P. Vasseur, F. Meng, L. Robillard, On the periodic conditions to simulate mixed convection heat transfer in horizontal channels, Numer. Heat Transfer A 27 (1995) 461–472.
[7] O. Aydin, W.J. Yang, Natural convection in enclosures with localized heating from below and symmetrical cooling from sides, J. Numer. Methods Heat Fluid Flow 10 (2000) 518–529.
[8] R. Ben Yedder, E. Bilgen, Turbulent natural convection in a square enclosure bounded by a solid wall with localized heating, Heat Mass Transfer 35 (1999) 401–408.
[9] O. Aydin, A. Unal, T. Ayhan, Natural convection in rectangular enclosure heated from one side and cooled from the ceiling, Int. J. Heat Mass Transfer 42 (1999) 2345–2355.
[10] M.M. Ganzarolli, L.F. Milanez, Natural convection in rectangular enclosures heated from below and symmetrically cooled from the sides, Int. J. Heat Mass Transfer 38 (1995) 1063–1073.
[11] P. Poulikakos, Natural convection in a confined fluid-filled space driven by a single vertical wall with warm and cold regions, J. Heat Transfer 107 (1985) 867–876.
[12] I.E. Sarris, I. Lekakis, N.S. Vlachos, Natural convection in a 2D enclosure with sinusoidal upper wall temperature, Numer. Heat Transfer A 42 (2002) 513–530.
[13] S.V. Patankar, Numerical Heat Transfer and Fluid Flow, Hemisphere Publishing Corp., New York, 1980.
[14] R. Ben Yedder, Étude paramétrique de la convection laminaire et turbulente dans des espaces clos avec parois solides, Dissertation, Université de Montréal, Canada, 1995.
[15] D. de Vahl Davis, Natural convection of air in a square cavity: a benchmark solution, Int. J. Numer. Meth. Fluids 3 (1983) 249–264.
[16] D.C. Wan, B.S.V. Patnaik, G.W. Wei, A new benchmark quality solution for the buoyancy-driven cavity by discrete singular convolution, Numer. Heat Transfer B 40 (2001) 199–228.